

# Analytic Model inclusive Transformer for Resonant Converters based on Extended Fundamental Frequency Analysis for Resonant Converter-Design and Optimisation

Jürgen Biela \* Non-member  
Johann W. Kolar \*\* Member

**Abstract** – The series-parallel resonant converter and its magnetic components are analysed by extended fundamental frequency techniques. The proposed model allows an easy design of the resonant circuit and the integrated transformer and the calculation of the losses of all components of the converter. The purpose of the presented analytic model is an optimisation of the converter system – minimising either the volume / power density or the losses of the converter (restriction: temperature rise). Moreover, the presented equations also include a ZCS condition for one leg of the converter, the control of the converter by the frequency *and* duty cycle and a load model with offset voltage. The proposed analytic model is validated by simulation as well as by experimental results.

**Keywords:** fundamental frequency analysis, transformer design, reluctance model, resonant converter, integrated transformer, optimization

## List of Symbols

$V_{IN}$	DC input voltage
$V_{AB}$	Converter output voltage
$V_{AB(1)}$	Fundamental component of $V_{AB}$
$V_{OUT}$	Output voltage
$V_{CP}$	Voltage across $C_P$
$V_{CP(1)}$	Fundamental component of $V_{CP}$
$V_{off}$	Offset voltage of load (cf. Fig. 1)
$C_S$	Series capacitor
$L_S$	Resonant inductor
$C_P$	Parallel capacitor
$I_P$	Primary current
$I_S$	Secondary current
$I_R$	Rectifier input current
$I_{R(1)}$	Fundamental component of $I_R$
$I_{OUT}$	Output current
$\omega$	Angular switching frequency
$Z$	Fundamental frequency impedance of the resonant circuit with load

$Z_{CpR}$	Fundamental frequency impedance of $C_P$ in parallel with the rectifier
$\alpha$	Angle between resonant current $I_S$ zero-crossing and start of rectifier commutation
$\beta$	Angular duration of zero voltage state in discontinuous parallel capacitor voltage waveform
$D$	Duty cycle
$N_P$	Number of primary turns
$N_S$	Number of secondary turns
$R$	Load resistance
$R_V$	Internal resistance of voltage source $V_{AB(1)}$ (cf. Fig. 5)
$\mathcal{R}_{M1}$	Magnetic reluctance of the transformer leg carrying the primary winding
$\mathcal{R}_{M2}$	Magnetic reluctance of the transformer leg carrying the secondary winding
$\mathcal{R}_\sigma$	Magnetic reluctance of the leakage path (including air gap)

## 1. Introduction

Applying resonant DC-DC converters can help to reduce the switching losses and / or to raise the switching frequency of the power switches. On this account the overall system size in many industrial applications, e.g., telecom power supplies [1], high voltage generators [2] or inductive heating [3] could be reduced and the power density could be increased. Especially, the series-parallel resonant converter, **Fig.1**, is a promising converter structure since it combines the advantages of the series resonant converter and the parallel resonant converter. On the one hand the resonant current decreases with the decrease of the load and the converter can be regulated at no load and on the other hand good part-load efficiency can be achieved [4 & 5]. Furthermore, the converter is naturally short circuit proof.

During the design of a resonant converter one has to determine for example the values of the resonant circuit elements ( $C_S$ ,  $L_S$  and  $C_P$ ), the turns ratio and the number of primary turns so that the

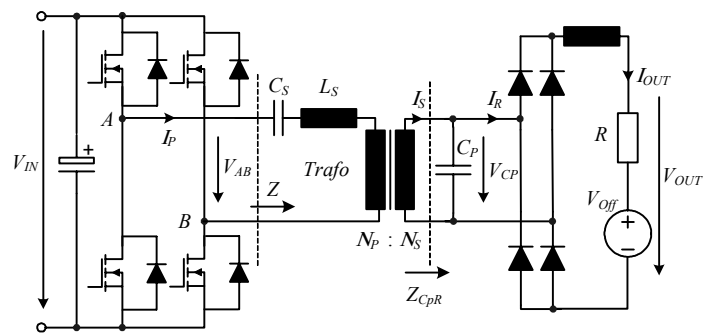


Fig. 1. Series-parallel resonant DC-DC converter

design constraints (temperature rise, operating frequency...) are met for the given specifications (input voltage, output power, load...). In order to find the values for the components which lead to an optimal design (optimal with respect to the given design aim – e.g. minimal converter volume, maximal efficiency, minimal costs...) one needs an automatic optimisation procedure. A possible flowchart for such an optimisation procedure is shown in **Fig. 2**. First, the specifications of the application and the initial values of the resonant circuit elements are fed into the analytic model of the resonant converter. Within the model the operating frequency,

\* Power Electronic Systems Laboratory, ETH Zürich, [biela@lem.ee.ethz.ch](mailto:biela@lem.ee.ethz.ch) Physikstrasse 3, CH-8092 Zürich, Switzerland

\*\* Power Electronic Systems Laboratory, ETH Zürich, [kolar@lem.ee.ethz.ch](mailto:kolar@lem.ee.ethz.ch) Physikstrasse 3, CH-8092 Zürich, Switzerland  
Homepage: [www.pes.ee.ethz.ch](http://www.pes.ee.ethz.ch)

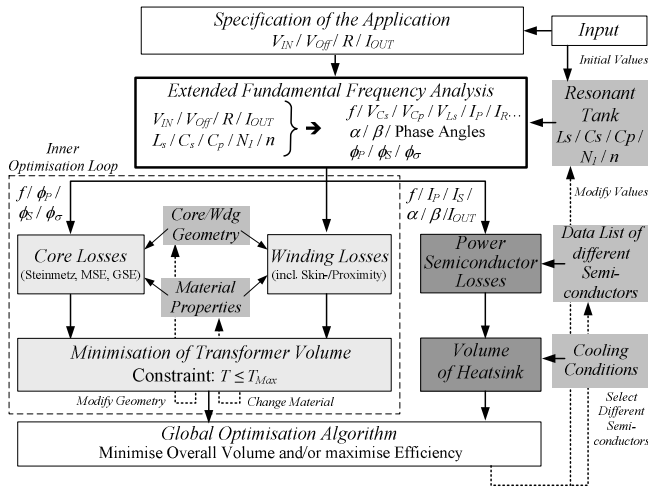


Fig. 2. Workflow of system optimisation procedure.

all voltages and currents of the converter inclusive phase shift and also the flux values in the transformer are computed. With this information the design of the transformer is optimised in an inner optimisation loop (cf. Fig. 2) so that the resulting transformer volume is minimal. In parallel the volume of the heatsink for the power semiconductors is calculated using the semiconductor losses and an analytic thermal heatsink model. The resulting volumes are fed into the global optimisation algorithm which varies the resonant circuit elements, the cooling conditions and the parameters of the semiconductors until a minimal overall converter volume is obtained.

For the described optimisation procedure an accurate model for the resonant converter is needed, which must not be too complicated in order to limit the computation time. The used model is based on the extended fundamental frequency analysis which is explained in principle in the following.

The resonant circuit of the series-parallel resonant converter is fed by a square wave input voltage  $V_{AB}$  which usually has a varying frequency and duty cycle. In order to achieve a ZVS condition in one leg of the converter and to prevent a MOSFET from a hard turn-off of a diode the operating frequency of the converter has to be always above the resonant frequency of the resonant circuit which is dependent on the load of the converter [2]. Furthermore, the amplitude of the resonant current for operation at light load must be large enough to discharge/charge the output capacitances of the MOSFETs. This could be always achieved by a proper

choice of the value of the parallel capacitor  $C_p$ .

The square wave input voltage is filtered by the resonant circuit so that the current in the resonant components is almost sinusoidal as shown in Fig. 3a. Neglecting the small harmonics of the resonant current the analytic calculation of the resonant converter can be done by simple AC circuit analysis where the square wave input voltage  $V_{AB}$ , the square wave rectifier input current  $I_R$  and the distorted voltage across the parallel capacitor  $V_{CP}$  are represented by their respective fundamental components. This method was proposed in [5].

Under heavy load conditions, however, the voltage waveform of the parallel capacitor  $V_{CP}$  is clamped by the output current to zero for a certain period of time, period  $\beta$  in Fig. 6(b), which leads to a discontinuous and very distorted parallel capacitor voltage  $V_{CP}$ . Under these conditions the standard fundamental frequency analysis is inaccurate. Therefore, the authors of [6] proposed an extended fundamental frequency analysis which accounts for the discontinuous capacitor voltage under heavy load conditions. This method uses two different models of the resonant converter – one for the continuous capacitor voltage mode (CCV) and one for the discontinuous capacitor voltage mode (DCV) and yields quite accurate results for all operating conditions (light, part, and heavy load). The equations of this model are based on the assumption of a negligible ripple of the output current.

With this analytic model the design of the resonant circuit including the voltage transfer ratio of the transformer could be performed quite accurately. The design of the transformer itself, however, is still elaborate since the current respectively voltage waveforms and their phase relation for the primary and secondary windings are required in order to be able to calculate the flux distribution within the core. This is particularly true if the series inductance is realised by the leakage inductance of the transformer which is increased by a magnetic shunt [7-10]. Depending on the winding geometry/core structure the three flux parts – primary linked flux, secondary linked flux and leakage flux – add or subtract in the different legs of the transformer where the absolute values and the phase relations of the fluxes have to be considered. Especially in the magnetic shunt the phase relations between the different flux parts must be considered in order to design the magnetic device properly.

For this reason the analytic model proposed in [6] is extended in this paper by a magnetic reluctance model of the transformer including the series inductance which is realised by the leakage inductance of the transformer. In Fig. 5 the series-parallel resonant converter with the reluctance model is shown. The presented reluctance model represents a simple E-core transformer where the

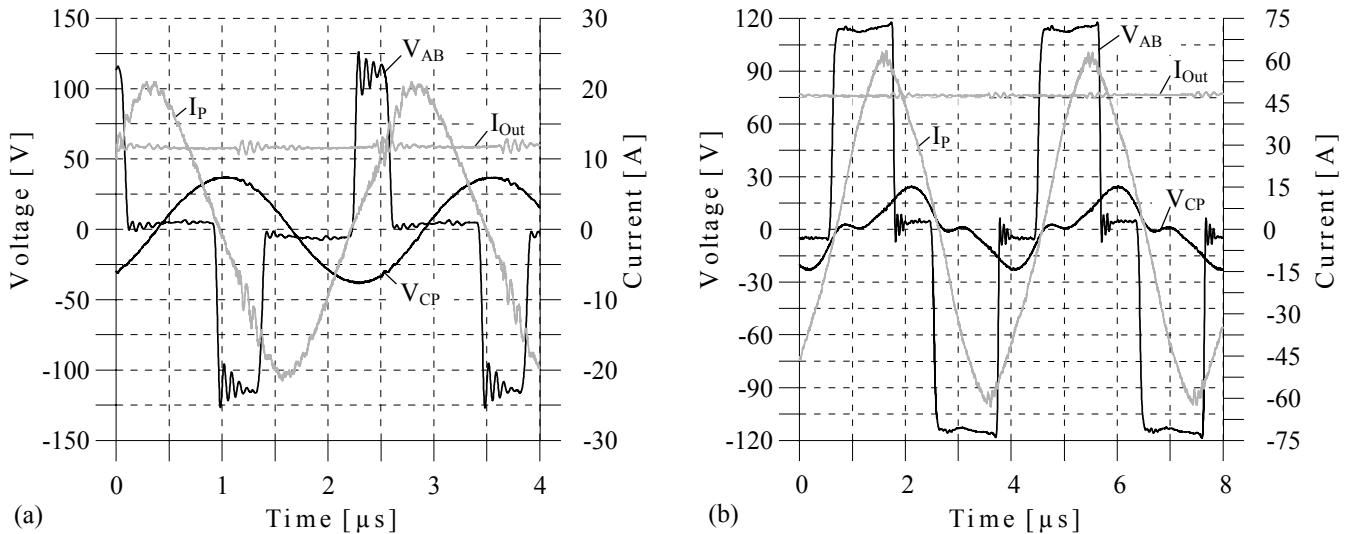


Fig. 3. (a) Measured converter output voltage  $V_{AB}$ , primary current  $I_P$ , output current  $I_{Out}$  and parallel capacitor voltage  $V_{CP}$  in continuous capacitor voltage mode CCV (light load –  $V_{IN}=320$ ,  $U_{Off}=0$ ,  $R_L=1.7\Omega$ ). (b) The same waveforms as for (a) but for discontinuous capacitor voltage mode (heavy load –  $R_L=0.2\Omega$ )

windings are placed on the two outer legs of the core and the magnetic shunt / leakage path is implemented by the centre leg (Fig. 4) but basically every core geometry and winding structure could be modelled in this way. The series inductance is controlled by the air gap in the centre leg. The derivation of the reluctance model is shortly presented in **section 2** before the analytic equations for the series-parallel resonant circuit including the reluctance model are presented in **section 3**.

There, the equations of [6] are also extended for an operation mode where one leg of the converter is always switched at the zero crossing of the resonant current  $I_p$  (Fig. 7). This is a known method to reduce the switching losses of the converter. Furthermore, the control of the output voltage/current by the duty cycle *and* the switching frequency is described by the extended set of equations which are presented in section 3.

After the derivation of the model the analytic results are validated by circuit simulations using SIMPLORER™ and measurements on different prototypes. The results of the comparison and the discussion are presented in **section 4** where also some results of the automatic optimisation procedure are presented. Finally, a conclusion and topics of future research are given in **section 5**.

## 2. Magnetic Circuit Model

In the following a short summary of magnetic circuit models based on [11] and the derivation of the equations which are applied in the calculations in section 3 is given.

By means of magnetic circuit models Ampere's law is simplified so that the line and surface integral do not have to be evaluated in order to find the flux distribution within the magnetic core. This simplification is based on the following two assumptions. Firstly, the absolute value of the magnetic field  $\vec{H}$  is constant in a given volume and secondly, the direction of the magnetic field  $\vec{H}$  is aligned with the direction of the path of integration. With this assumptions Ampere's law simplifies to

$$\oint_l \vec{H} \cdot d\vec{l} = \iint_S \vec{J} \cdot d\vec{s} \Rightarrow H \cdot l = N \cdot I. \quad (1)$$

Applying the relationship between the flux density  $B$  and the magnetic field and the definition of the flux yields

$$\left. \begin{aligned} \vec{B} &= \mu_0 \cdot \mu_r \cdot \vec{H} \\ \Phi &= B \cdot A_e \end{aligned} \right\} \Phi \cdot \frac{l}{\mu \cdot A_e} = \Phi \cdot \mathfrak{R} = N \cdot I. \quad (2)$$

The quantity  $\mathfrak{R}$  is referred to as the magnetic reluctance (of the path  $l$ ) and the product  $N \cdot I$  is known as the magneto motive force (mmf). Equation (2) represents Ohm's law for magnetic circuits which is the magnetic analogue to the Ohm's law for electric circuits:  $R \cdot I = U$ , i.e. the flux corresponds to the current and the mmf to the voltage. With this equation and above mentioned assumptions also Kirchhoff's voltage law (VL) and current law (CL) can be applied to the magnetic circuit.

$$\begin{aligned} \text{VL: } N \cdot I &= \Phi \cdot (\mathfrak{R}_1 + \mathfrak{R}_2 + \dots + \mathfrak{R}_n) && (\text{for a given path}) \\ \text{CL: } \Phi_1 + \Phi_2 + \dots + \Phi_n &= 0 && (\text{for a given node}) \end{aligned} \quad (3)$$

Thus, by solving the system equation of the magnetic circuit the flux distribution in the core can be calculated. The application of Faraday's law then leads to the induced voltage

$$V = \frac{d\Psi}{dt} = N \cdot \frac{d\Phi}{dt}. \quad (4)$$

Assuming that the flux varies sinusoidally with time (4) can be rewritten as

$$\underline{V} = j \cdot \omega \cdot \underline{\Phi}. \quad (5)$$

In (5)  $\underline{V}$  is the complex voltage vector and  $\underline{\Phi}$  is the complex vector of the magnetic flux.

The above mentioned assumptions for applying magnetic circuit theory are approximately fulfilled in regions of high permeability

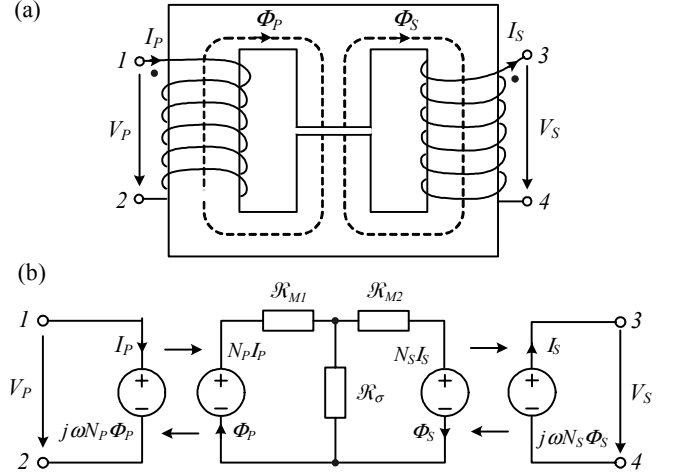


Fig. 4. (a) Transformer on E-core (the middle leg carries the leakage flux) (b) Magnetic circuit model of the transformer

(e.g. ferrite core) if, among other things, the skin effect of magnetic fields is neglected for HF-applications. Usually, in air gaps the magnitude of the magnetic field is not constant over the cross section because of fringing flux. For calculating the magnetic reluctance of air gaps empirical and FEM-based models [12, 13 & 14] have been proposed. Here the flux density / exact magnetic field distribution is not important (no losses are generated in the gap) but only the overall magnetic reluctance seen by the flux is needed for the calculations.

In principle, it is possible to model the magnetic device very accurately with magnetic reluctances (with an increasing number of modelled magnetic paths) but usually a quite simple model is enough for getting reasonably exact results. In **Fig. 4(a)** an E-core with two windings on its outer legs and the definition of the directions for the quantities is given. With this winding structure the centre leg carries the leakage flux ( $\Phi_p - \Phi_s$ ) and the leakage inductance is adjusted to the needed value by the air gap in this leg. Below, in **Fig. 4(b)**, the appropriate magnetic circuit model is given for sinusoidal fluxes.

Applying the magnetic analogue of Kirchhoff's voltage law, (3), to the two loops of the magnetic circuit in Fig. 4(b) yields the following two equations

$$\begin{aligned} N_p I_p &= \mathfrak{R}_{M1} \Phi_p + \mathfrak{R}_{\sigma} \cdot (\Phi_p - \Phi_s) \\ N_s I_s &= -(\mathfrak{R}_{M2} \Phi_s + \mathfrak{R}_{\sigma} \cdot (\Phi_s - \Phi_p)) \end{aligned} \quad (6)$$

Solving these equations for the flux values and using  $U = N \cdot d\Phi/dt = L \cdot dl/dt$  leads to the following relations between the magnetic reluctances and the inductances.

$$\begin{aligned} L_1 &= \frac{N_p^2 \cdot (\mathfrak{R}_{M2} + \mathfrak{R}_{\sigma})}{\mathfrak{R}_{M1} \mathfrak{R}_{M2} + \mathfrak{R}_{M1} \mathfrak{R}_{\sigma} + \mathfrak{R}_{\sigma} \mathfrak{R}_{M2}} \\ L_2 &= \frac{N_s^2 \cdot (\mathfrak{R}_{M1} + \mathfrak{R}_{\sigma})}{\mathfrak{R}_{M1} \mathfrak{R}_{M2} + \mathfrak{R}_{M1} \mathfrak{R}_{\sigma} + \mathfrak{R}_{\sigma} \mathfrak{R}_{M2}} \\ L_{\sigma(P)} &= \frac{N_p^2}{\mathfrak{R}_{M1} + \mathfrak{R}_{\sigma}} L_{\sigma(S)} = \frac{N_s^2}{\mathfrak{R}_{M2} + \mathfrak{R}_{\sigma}} \end{aligned} \quad (7)$$

The inductance  $L_1$  can be measured at the primary side when the secondary is left open and  $L_2$  is the same for the secondary side. Additionally, the equation for the complete leakage inductance is given - one referred to the primary side  $L_{\sigma(P)}$  and one to the secondary side  $L_{\sigma(S)}$ . With the above equations the analytic model for the series-parallel resonant converter including the transformer could be set up in the following section.

## 3. Analysis of the Extended Model

As already mentioned the following considerations for the series-parallel resonant converter shown in **Fig. 5** are partly based

on the fundamental frequency analysis proposed in [6]. The method of [6] has been extended by a reluctance model for the transformer with its leakage inductance, a ZCS condition for one leg and the control by frequency *and* duty cycle. As far as possible and reasonable the notation used in [6] has been retained.

The calculations are based on the assumptions that both the primary resonant current  $I_P$  and the secondary resonant current  $I_S$  are sinusoidal, that the output current is constant and that the components are ideal. The major procedure of the analysis is to determine the fundamental frequency impedance  $\underline{Z}_{CPR}$  of the parallel connection of  $C_P$  and the rectifier at first. With this impedance the input impedance  $\underline{Z}$  of the resonant circuit, seen by the converter / voltage source  $V_{AB}$ , could be calculated. In the impedance  $\underline{Z}$  also the reluctance model of the transformer is included. In the next step two equations can be set up. The first one describes the relation between the phase shift of the primary current  $I_P$  and  $\underline{V}_{AB(1)}$  (Fig. 7), which is determined on the one hand by the duty cycle  $D$  and on the other hand by  $\underline{Z}$ . The second expression relates the output voltage  $V_{OUT}$  of the converter to the load voltage which is given by the load characteristic ( $V_{OFF}$  &  $R$ ) and the output current  $I_{OUT}$ . These two equations together with one (CCV) or two (DCV) additional equations describe the behaviour of the system. The duty cycle  $D$  and the output current / voltage now can be calculated numerically for a given frequency  $f$  and load characteristic ( $V_{OFF}$  &  $R$ ) or vice versa.

**3.1 Fundamental frequency impedance  $\underline{Z}_{CPR}$**  In the following the impedance  $\underline{Z}_{CPR}$  is calculated for the DCV (Fig. 6(b)) by first considering the fundamental component of the rectifier input current  $\underline{I}_{R(1)}$  (cf. Fig. 5) (~(1) in [6]).

$$\begin{aligned} \underline{I}_{R(1)} &= \frac{2j}{\pi} \left[ \int_{\alpha}^{\alpha+\beta} I_S \cdot \sin\theta \cdot e^{-j\theta} d\theta + \int_{\alpha+\beta}^{\alpha+\pi} I_{OUT} \cdot e^{-j\theta} d\theta \right] \\ \underline{I}_{R(1)} &= \frac{2}{\pi} \left[ \frac{I_S}{4} \cdot (2\beta - je^{-2j\alpha} \cdot (e^{-2j\beta} - 1)) + \right. \\ &\quad \left. + I_{OUT} \cdot (1 + e^{-j\beta}) e^{-j\alpha} \right] \end{aligned} \quad (8)$$

Since the resonant current on the secondary  $I_S$  is assumed to be sinusoidal the fundamental component of the capacitor voltage  $\underline{V}_{CP(1)}$  could simply be calculated by AC circuit analysis and is given by (~(2) in [6])

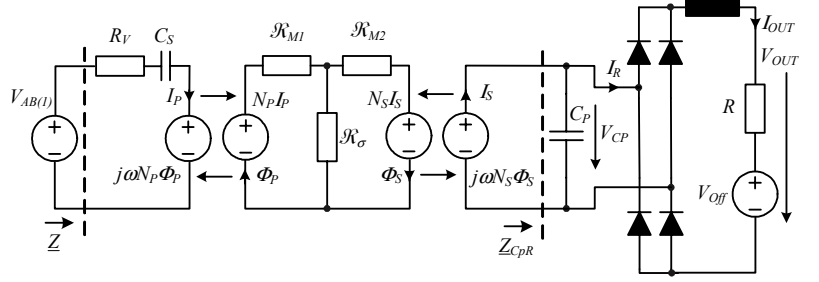


Fig. 5. Series-parallel resonant converter with reluctance model of the transformer. The converter output voltage  $V_{AB}$  is represented by its fundamental component  $V_{AB(1)}$ .

$$\underline{V}_{CP(1)} = \frac{I_S - \underline{I}_{R(1)}}{j\omega C_P} \quad (9)$$

Dividing the capacitor voltage  $\underline{V}_{CP(1)}$  by the sinusoidal secondary resonant current  $I_S$  yields the fundamental component of the secondary side impedance  $\underline{Z}_{CPR}$  (~(3) in [6])

$$\begin{aligned} \underline{Z}_{CPR} &= \frac{\underline{V}_{CP(1)}}{I_S} = \\ &= \frac{2\pi - 2\beta + je^{-2j\alpha} \cdot (e^{-2j\beta} - 1) - 4 \frac{I_{OUT}}{I_S} (1 + e^{-j\beta}) e^{-j\alpha}}{2j\pi\omega C_P} \end{aligned} \quad (10)$$

The impedance  $\underline{Z}_{CPR}$  for the CCV is obtained by setting  $\beta = 0$  in (10).

**3.2 Continuous Capacitor Voltage Mode (CCV)** In the CCV the value of the resonant current  $I_S$  at the angle  $\alpha$  (where  $V_{CP}$  falls to zero) is larger than  $I_{OUT}$ . The difference between the resonant current  $I_S$  and the output current  $I_{OUT}$  charges the capacitor  $C_P$ . Thus the time response of the capacitor voltage is given by (~(5) in [6])

$$\begin{aligned} V_{CP}(\theta) &= \frac{1}{\omega C_P} \int_{\alpha}^{\theta} (I_S \cdot \sin\varphi - I_{OUT}) d\varphi \\ &= \frac{I_S (\cos\alpha - \cos\theta) - I_{OUT}(\theta - \alpha)}{\omega C_P} \end{aligned} \quad (11)$$

for  $\alpha \leq \theta \leq \alpha + \pi$ . Since the capacitor voltage is periodic for steady state operation it must fall to zero at the end of each cycle.

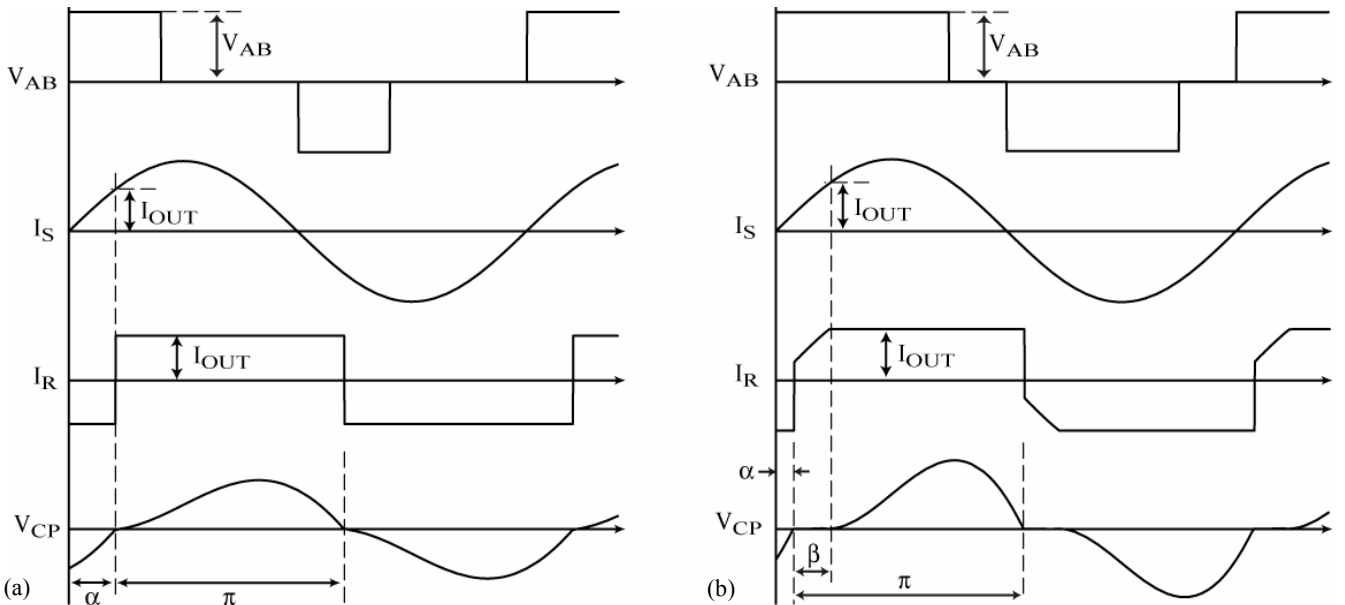


Fig. 6. (a) Converter output voltage  $V_{AB}$ , primary current  $I_P$ , rectifier current  $I_R$  and parallel capacitor voltage  $V_{CP}$  in continuous capacitor voltage mode. (b) The same waveforms as for (a) but for discontinuous capacitor voltage mode (assumption: magnetizing current  $I_M = 0$ )

Evaluating (11) under this condition yields an expression for  $\alpha$  (~(6) in [6]).

$$V_{CP}(\alpha + \pi) = 0 \Rightarrow$$

$$\alpha = \arccos\left(\frac{I_{OUT} \cdot \pi}{2I_S}\right) \quad (12)$$

Furthermore, the average value of the capacitor voltage  $V_{CP}$  must be equal to the output voltage  $V_{OUT}$  because the volt-seconds across the output inductor must be balanced. Calculating the average value of  $V_{CP}$  according to (11) and using (12) for substituting  $I_{OUT}$  results in (~(7) in [6])

$$V_{OUT} = \frac{1}{\pi} \int_{\alpha}^{\alpha+\pi} V_{CP}(\varphi) d\varphi = \frac{2I_S \sin \alpha}{\pi \omega C_P} \quad (13)$$

Another equation for  $\alpha$  may be obtained by inserting the output voltage  $V_{OUT} = V_{OFF} + R \cdot I_{OUT}$  (equal to the load voltage) in (13) and solving for  $\sin(\alpha)$ . The resulting equation must be divided by (12) which has to be solved for  $\cos(\alpha)$  first. This results in (14)

$$\alpha = \arctan\left(\frac{\omega C_P \cdot (V_{OFF} + R \cdot I_{OUT})}{I_{OUT}}\right) \quad (14)$$

which is the first system equation for the CCV (~(8) in [6]). By setting  $\beta = 0$  in (10) the impedance  $\underline{Z}_{CpR}$  for the CCV is obtained which may be simplified by substituting  $I_{OUT}/I_S$  using (12) (~(9) in [6])

$$\underline{Z}_{CpR} = \frac{1-8/\pi^2 \cdot e^{j\alpha} \cdot \cos \alpha}{j\omega C_P} \quad (15)$$

With (6), i.e. the description of the transformer (incl.  $L_S$ ) and (16)

$$\underline{L}_S = \frac{V_S}{\underline{Z}_{CpR}} = \frac{j\omega \cdot N_2 \cdot \Phi_S}{\underline{Z}_{CpR}} \quad (16)$$

the flux  $\Phi_P$  and therewith the primary voltage  $\underline{V}_P (= j\omega N_1 \Phi_P)$  of the transformer could be calculated as a function of  $\underline{L}_P$  and  $\underline{Z}_{CpR}$ . Applying Kirchoff's voltage law to the most left mesh in Fig. 5 yields

$$\underline{V}_{AB(l)} = R_V \cdot \underline{I}_P + \frac{\underline{L}_P}{j\omega C_S} + j\omega \cdot N_1 \cdot \underline{\Phi}_P$$

$$\Rightarrow \underline{Z} = \frac{\underline{V}_{AB(l)}}{\underline{I}_P} \quad (17)$$

Dividing  $\underline{V}_{AB(l)}$  by the primary current  $\underline{I}_P$  results in the fundamental frequency input impedance  $\underline{Z}$  of the resonant circuit. By means of the phase of the impedance  $\underline{Z}$  the second system equation for the CCV could be set up. The phase shift between the fundamental component of the input voltage  $\underline{V}_{AB(l)}$  and the resonant current  $\underline{I}_P$  is on the one hand determined by the phase of  $\underline{Z}$ . On the other hand this phase shift is determined by the ZCS condition (one leg is always switched at the zero crossing of the resonant current  $\underline{I}_P$ ) and the duty cycle  $D$  (cf. Fig. 7). Equating both conditions yields

$$\frac{\pi}{2} (1-D) = \arctan\left(\frac{\text{Im}(\underline{Z})}{\text{Re}(\underline{Z})}\right) \quad (18)$$

With the absolute value of the impedance  $\underline{Z}$  the absolute value of the primary resonant current  $\underline{I}_P$  could be calculated as

$$|\underline{I}_P| = \frac{4}{\pi} V_{IN} \cdot \frac{\cos(\pi/2 \cdot (1-D))}{|\underline{Z}|} \quad (19)$$

Now the absolute value of  $\underline{L}_S$  could be calculated with equations (6) by substituting  $\underline{L}_P$  by (19) and  $\underline{\Phi}_S$  by means of (16). The resulting equation for  $|\underline{L}_S|$  is used for calculating the output voltage  $V_{OUT}$  by (13). This output voltage must be equal to the load voltage which is given by the load characteristic and the output current  $I_{OUT}$ .

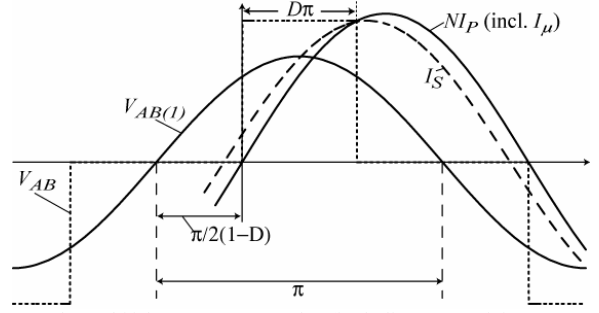


Fig. 7. Phase shift between  $V_{AB(l)}$  and  $I_P$  (including magnetizing current  $I_\mu$ ) and between  $I_S$  and  $I_P$  (due to  $I_\mu$ ).

$$V_{OFF} + R \cdot I_{OUT} = \frac{2|\underline{L}_S| \sin \alpha}{\pi \omega C_P} \quad (20)$$

Equation (20) is the third system equation for the CCV. By solving the three system equations [(14), (18) and (20)] numerically the output voltage  $V_{OUT}$ , the output current  $I_{OUT}$ , the duty cycle  $D$  and  $\alpha$  can be calculated for a given frequency  $f$  and load characteristic  $V_{OFF}$  &  $R$  or vice versa.

The CCV occurs if the resonant current  $I_S$  is larger than the output current  $I_{OUT}$  when the capacitor voltage  $V_{CP}$  falls to zero at the angle  $\alpha$ . Therefore, the limit for the CCV is given by

$$I_S \sin \alpha > I_{OUT} \xrightarrow{\text{Eqn. 13}} \frac{\omega C_P (V_{OFF} + R I_{OUT})}{I_{OUT}} > \frac{2}{\pi} \quad (21)$$

**3.3 Discontinuous Capacitor Voltage Mode (DCV)** In contrast to the CCV the value of the resonant current  $I_S$  at the angle  $\alpha$  (where  $V_{CP}$  falls to zero) is smaller than  $I_{OUT}$  in the DCV. As long as the resonant current  $I_S$  is smaller than  $I_{OUT}$  the capacitor voltage  $V_{CP}$  is clamped to zero by the negative difference between  $I_S$  and  $I_{OUT}$   $[-(I_S - I_{OUT})]$  which flows through the rectifier diodes. From the angle  $\beta$  on  $I_S$  is larger than  $I_{OUT}$  and in the same manner as in CCV the positive difference between the currents  $(I_S - I_{OUT})$  charges the capacitor  $C_P$ . Thus the capacitor voltage is given by (~(12) in [6])

$$\alpha \leq \theta \leq \alpha + \beta$$

$$V_{CP}(\theta) = 0$$

$$\alpha + \beta \leq \theta \leq \alpha + \pi \quad (22)$$

$$V_{CP}(\theta) = \frac{1}{\omega C_P} \int_{\alpha+\beta}^{\theta} (I_S \cdot \sin \varphi - I_{OUT}) d\varphi$$

$$V_{CP}(\theta) = \frac{I_S (\cos(\alpha + \beta) - \cos \theta) - I_{OUT} (\theta - \alpha - \beta)}{\omega C_P}$$

Again, the average value of the capacitor voltage  $V_{CP}$  must be equal to the output voltage. After carrying out the integration the expression could be simplified by using  $I_S \sin(\alpha + \beta) = I_{OUT}$ . The result of this operation is given in (~(14) in [6])

$$V_{OUT} = \frac{1}{\pi} \int_{\alpha}^{\alpha+\pi} V_{CP}(\varphi) d\varphi$$

$$= \frac{(\pi - \beta) \cdot I_S \cdot [\cos(\alpha + \beta) + \sin(\alpha)]}{\pi \omega C_P} +$$

$$+ \frac{I_{OUT} \cdot (1 + \beta\pi - \beta^2/2 - \pi^2/2)}{\pi \omega C_P} \quad (23)$$

In the DCV two equations are needed for calculating the angles  $\alpha$  and  $\beta$ . One is obtained by setting  $V_{CP}$  equal to zero at the end of every half cycle  $V_{CP}(\alpha + \pi) = 0$  (~(15) in [6])

$$\cos(\alpha + \beta) + \cos(\alpha) + (\beta - \pi) \cdot \sin(\alpha + \beta) = 0 \quad (24)$$

The second one is given by  $I_S \sin(\alpha + \beta) = I_{OUT}$  which relates the angles  $\alpha$  and  $\beta$  with the absolute value of the resonant current on the secondary  $I_S$  and with the output current  $I_{OUT}$ . In order to eliminate  $I_S$  this equation is put in (23) which is set equal to the load voltage  $V_{OUT} = V_{Off} + R \cdot I_{OUT}$ . This results in  $(\sim(15))$  in [6].

$$(\pi - \beta) \cdot \cos(\alpha + \beta) + \sin(\alpha) + \sin(\alpha + \beta) \cdot \left[ \left( 1 + \beta\pi - \frac{\pi^2 + \beta^2}{2} \right) - \left( \frac{V_{Off}}{I_{OUT}} + R \right) \cdot (\omega\pi C_p) \right] = 0. \quad (25)$$

The third and fourth system equation are given by (18) and (20) which are derived {by (16), (17) and (19)} in the same manner as described for the CCV except for setting  $\beta = 0$  in  $Z_{CpR}$  in (16).

Due to the offset voltage of the load characteristic (25) is dependent on the output current  $I_{OUT}$ . Consequently, the two nonlinear equations for the angles  $\alpha$  and  $\beta$  {(24) and (25)} must be solved numerically together with (18) and (20).

Instead of applying the described reluctance model for the magnetic device for calculating the flux distribution in the core it is also possible to use the standard network model equations of a transformer

$$\begin{aligned} V_p &= j\omega L_1 I_p + j\omega M I_s \\ V_s &= j\omega M I_p + j\omega L_2 I_s \end{aligned} \quad (26)$$

and calculate the flux through the primary and the secondary winding by

$$\underline{\phi}_p = \frac{1}{j\omega N_p} \cdot \underline{U}_p \quad \text{and} \quad \underline{\phi}_s = \frac{1}{j\omega N_s} \cdot \underline{U}_s. \quad (27)$$

For simple transformer designs the leakage flux could be approximated by the difference of the primary and the secondary flux. This is, however, limited to standard transformer designs. More sophisticated transformers (e.g. integrated magnetic devices or transformers with two magnetic shunts and/or leakage flux in the window) can not be described by the network equations as accurately as with the description of the device by magnetic reluctances. Furthermore, the magnetic reluctances directly depend on the geometry of the device what could be used in an optimisation process of the converter. The values for  $L_1$ ,  $L_2$  and  $M$  in (26) must either be measured or calculated by a FEA and/or a reluctance model. Thus, the approach with reluctance models is directly based on the physics and the geometry of the device and therefore is used for the proposed calculation method.

#### 4. Validation of the Analytic Model

For validating the equations the results of the calculations are compared with simulation and measurement results in the following. First, the simulation results of a series-parallel resonant converter, which is operating in the CCV and the DCV, are compared with the analytic calculations. Thereafter, measurement and analytic results for a magnetically integrated transformer, which realises the series inductance of the resonant tank by its leakage inductance, are shown. Finally, measurement results for an electromagnetically integrated transformer are compared with the analytic calculations.

In **Fig. 8** the results for the operating frequency and the duty cycle of the analytic calculations and of the simulation of the series-parallel resonant converter are shown. The simulation is realised with SIMPLORER™ and includes a physical transformer model, where the flux values in the different legs of the transformer also can be simulated. The value of the resonant tank elements and the load are:

- Series inductance  $L_s = 12.5\mu\text{H}$
- Series capacitance  $C_s = 35\text{nF}$
- Parallel capacitance  $C_p = 110\text{nF}$
- Load:  $R = 0.04\Omega / V_{Off} = 20\text{V}$

For these values the converter is in the CCV mode for light load (app. up to 45A output current) and in the DCV mode for heavy

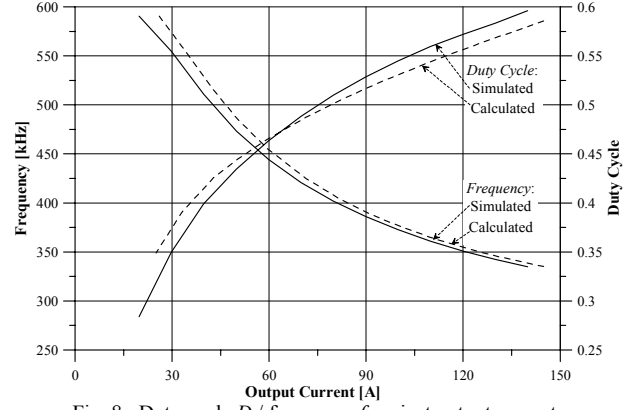


Fig. 8. Duty cycle  $D$  / frequency  $f$  against output current. *Solid lines*: results of simulations. *Broken lines*: predictions of proposed analytic model.

load. The crossover between the two analytic models describing the different modes is very smooth.

In **Fig. 9** the values for the flux through the primary and the secondary winding and the leakage flux are shown. As one can see the analytical results are in very good correspondence with the results of the simulation.

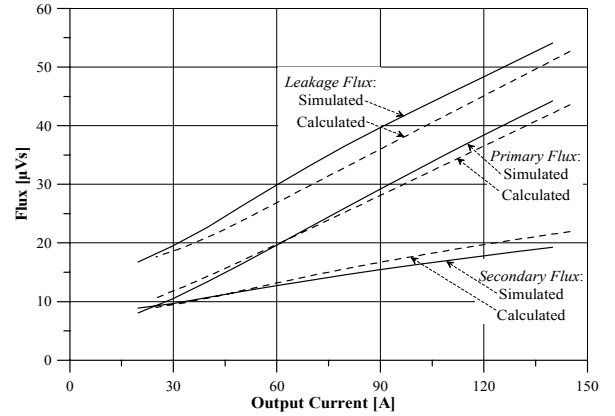


Fig. 9. Fluxes ( $|\Phi_p|$ ,  $|\Phi_s|$  and  $|\Phi_p + \Phi_s|$ ) in the three legs of the E-core against output current. *Solid lines*: results of simulations. *Broken lines*: predictions of proposed analytic model.

In the next step the analytic and the simulation results are compared with measurement results, which are obtained with the converter shown in **Fig. 10**. There, the resonant tank is built up with discrete elements except for the series inductance which is integrated in the transformer. The secondary winding of the transformer has a midpoint connection and its turn ratio is 14:2:2. The values of the resonant tank elements and the load are:

- Series inductance  $L_s = 37\mu\text{H}$
- Series capacitance  $C_s = 88\text{nF}$
- Parallel capacitance  $C_p = 348\text{nF}$
- Load:  $R = 0.27\Omega / V_{Off} = 0\text{V}$ .



Fig. 10. Prototype of a 5kW/500kHz series-parallel resonant converter with ZCS in one and ZVS in the other leg.

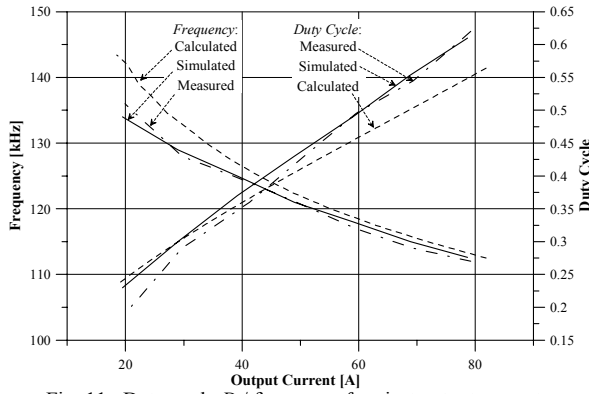


Fig. 11. Duty cycle  $D$  / frequency  $f$  against output current.  
*Solid lines:* results of simulations.  
*Broken lines:* predictions of proposed analytic model  
*Dot and dash line:* measurement results.

In **Fig. 11** the results for the operating frequency and for the duty cycle and in **Fig. 12/13** the results for the flux through the primary and the secondary winding and the leakage flux are given. There, the converter is just operating in the DCV due to the small value of the load resistance.

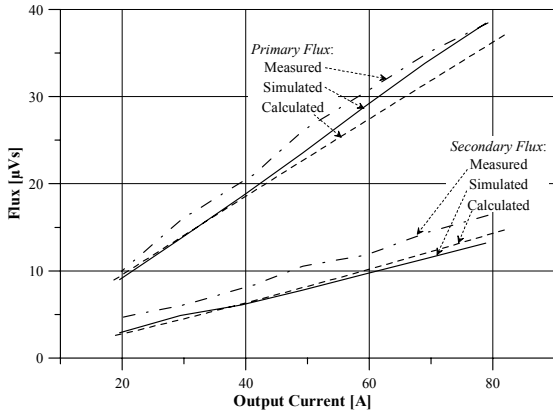


Fig. 12. Fluxes ( $|\Phi_p|$  and  $|\Phi_s|$ ) through the two windings against output current. *Solid lines:* results of simulations.  
*Broken lines:* predictions of proposed analytic model.  
*Dot and dash line:* measurement results.

The flux values can be measured by integrating the voltages across the windings. With this method the leakage flux is calculated as difference between the primary and the secondary flux. A more accurate method is to use a measurement winding (one turn) around the two legs of the core and the magnetic shunt and integrate the induced voltages. Therewith, the leakage flux could be measured directly.

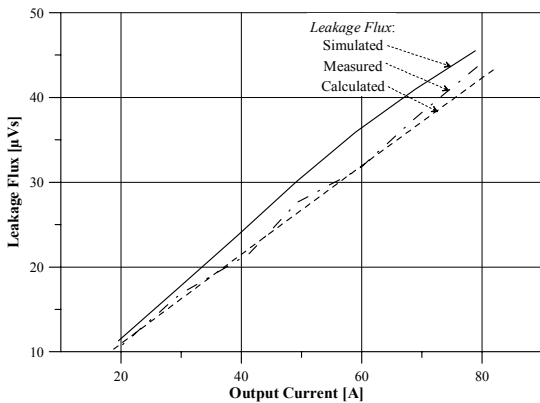


Fig. 13. Leakage Flux ( $|\Phi_p + \Phi_s|$ ) in the magnetic shunt of the E-core against output current. *Solid lines:* results of simulations. *Broken lines:* predictions of proposed analytic model. *Dot and dash line:* measurement results.

Again, the results for the analytic calculation, for the simulation and also for the measurement correspond very well.

Finally, the results for an electromagnetic integrated transformer shown in **Fig. 14** are presented. There, the series capacitance is realised by the primary winding and the parallel capacitance by the secondary winding. Moreover, the series inductance is implemented by increasing the leakage inductance of the transformer. The basic principles of integrating capacities and inductivities are explained in [7 - 10] and the design of the enclosing winding structure is presented in [10]. The values of the integrated resonant tank elements are:

- Series inductance  $L_s = 21 \mu\text{H}$
- Series capacitance  $C_s = 37 \text{nF}$
- Parallel capacitance  $C_p = 115 \text{nF}$ .

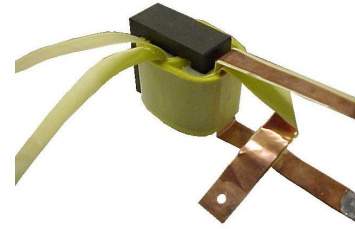


Fig. 14. Electromagnetically integrated transformer

With the electromagnetically integrated transformer the flux values in the different legs of the core must be measured with additional windings around the legs of the core (as described above). This is especially true for the primary winding since the measured voltage at the connections of the winding is the sum of the voltage across the series capacitance and the induced voltage which is not directly linked with the primary flux.

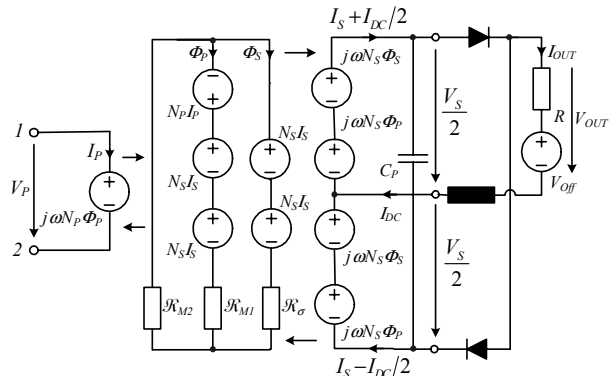


Fig. 15. Magnetic circuit diagram of the electromagnetically integrated transformer with rectifier and load

The reluctance model of the integrated transformer and the circuit diagram of the rectifier with load are given in **Fig 15**. The corresponding equations are given in (28).

$$\begin{aligned} N_p I_p &= \mathcal{R}_{M1} \Phi_p - \mathcal{R}_\sigma \Phi_s \\ 2N_s I_s &= -(\mathcal{R}_\sigma \Phi_s + \mathcal{R}_{M2} \cdot (\Phi_p + \Phi_s)) \end{aligned} \quad (28)$$

In **Fig. 16** the measured and calculated operating frequency and duty cycle against the output current are plotted and in **Fig. 17** the values for the primary, the secondary and the leakage flux are shown. Again, the converter is just operating in the DCV-mode due to the relation between the resonant tank elements and the load.

*Remark:* One leg of the converter is always switched at the zero crossing of the resonant current  $I_p$  (ZCS). In order to avoid for the complete load range that the anti-parallel diode of the MOSFET is turned off hardly the ZCS leg must be switched always a little bit before the zero crossing. This safety margin varies with the load current and also influences the actual switching frequency of the

converter. This effect is not included in the proposed analytic model and causes the relatively large deviation (approximately 7.5%) of the calculated result from the measured result for large output currents in Fig. 16.

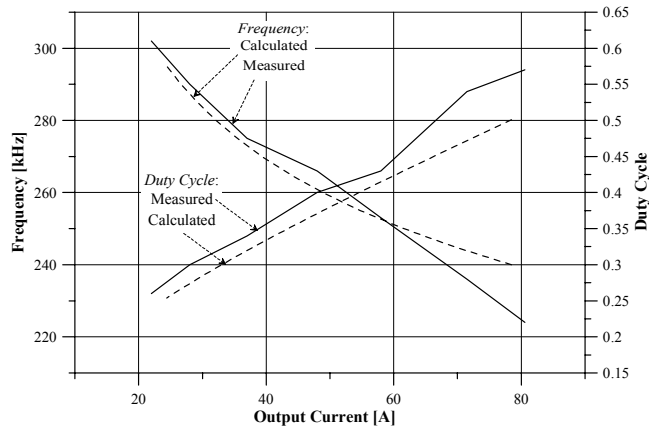


Fig. 16. Duty cycle  $D$  / frequency  $f$  against output current. *Solid lines*: measurement results. *Broken lines*: predictions of proposed analytic model

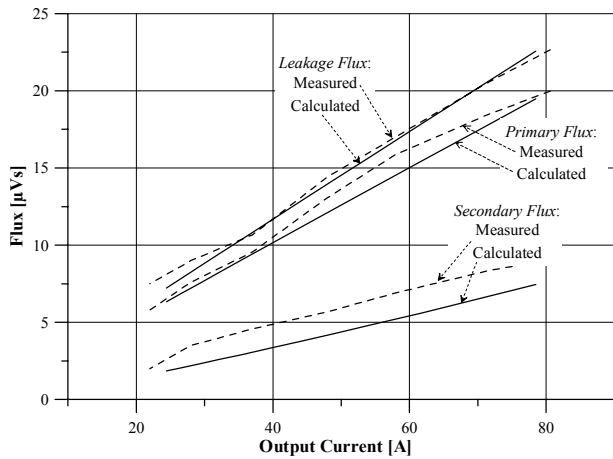


Fig. 17. Fluxes ( $|\Phi_S|$ ,  $|\Phi_P|$  and  $|\Phi_P + \Phi_S|$ ) in the different paths of the integrated core against output current. *Solid lines*: measurement results. *Broken lines*: proposed analytic model

The values predicted by the proposed calculation method are again in good correspondence with the measurement results.

As shown above the proposed analytic model for the series-parallel resonant converter predicts accurately the operating frequency, the duty cycle, all the voltages and currents (amplitude and phase) and also the flux values in the core if the resonant tank elements, the input voltage, the load current and the load are given (cf. Fig. 2). Furthermore, the model just consists just of a set of three equations for the CCV / four equations for the DCV which are solved numerically in order to calculate the operating point. The computation time is in the range of a few seconds (<30s on a Pentium IV, 2.8 GHz for DCV). Thus, the analytic model could be used in the proposed optimisation procedure (Fig.2).

The grey shaded area in Fig. 18 - where the volume of the resonant circuit (i.e. the volume of the capacitors plus the volume of the integrated transformer) against the operation frequency at full load is given - shows the region for the volume and the frequency which could be reached if the values of the components is varied within the following bounds:  $C_S = 20..250\text{nF}$  /  $C_P = 70..600\text{nF}$  /  $L_S = 1..10\mu\text{H}$ . This area is determined by varying the value of the series capacitance, the series inductance and the parallel capacitance within the given bounds and calculating the optimal volume of the converter for each fixed triple  $\langle C_S, C_P, L_S \rangle$  with the de-

scribed optimisation procedure (cg. Fig. 2 - except the "Global Optimisation Algorithm" which is replaced by a for-next-loop). Each cross in Fig. 18 marks a volume obtained for one triple  $\langle C_S, C_P, L_S \rangle$  whereby the number of primary and secondary turns is kept constant ( $N_1 = 14$  and  $N_2 = 2$ ). As one can see there is a distinct minimum of the volume close to 400kHz. Increasing or decreasing the operation frequency leads to an increasing volume. The values of the different parameters for the minimum volume calculated with the optimisation procedure are given in Table 1.

The presented result for the optimisation is based on the following data:

- Core material: *N87 from Epcos*
- Winding: *Foil winding / solid wire*
- Transformer: *Fixed power loss per surface area*  
(Core:  $1200\text{W/m}^2$  || Winding:  $2200\text{W/m}^2$ )
- Centre Tapped secondary winding (Fig. 14)
- MOSFETs: *APT50M75B2LFL from APT*
- Capacitors: *Reference B32671 series from Epcos*
- Cooling capacity of heatsink:  $200\text{W/dm}^3$

The "Global Optimisation Algorithm" of the optimisation procedure has been replaced by a for-next-loop in order to see the sensitivity of the minimum i.e. the penalty one has to pay if the designed values for the components of the resonant tank are not equal to the optimal ones.

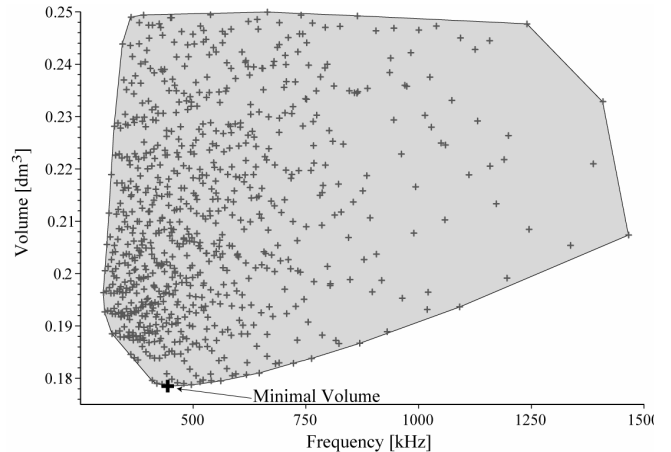


Fig. 18. Volume of the resonant circuit ( $C_S + C_P + L_S$  + transformer) for parameter range:  $C_S = 20..250\text{nF}$  /  $C_P = 70..600\text{nF}$  /  $L_S = 1..10\mu\text{H}$  /  $N_1 = 14$  /  $N_2 = 2$

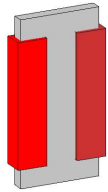
<b>Volume: 1.36dm<sup>3</sup> Efficiency: 93% Power Density: 2.85 kW/dm<sup>3</sup></b>		
	<i>Transformer:</i>	
	<ul style="list-style-type: none"> <li>• Width: 7.5 cm</li> <li>• Breadth: 1.8 cm</li> <li>• Height: 13.8 cm</li> <li>• Volume: 0.14 dm<sup>3</sup></li> <li>• Flux Density: 60 mT</li> </ul>	
<i>Operation Point:</i>		
<ul style="list-style-type: none"> <li>• Output Power: 3.9 kW</li> <li>• Output Current: 80 A</li> <li>• Nominal Frequency: 382 kHz</li> </ul>	<ul style="list-style-type: none"> <li>• Output Voltage: 48 V</li> <li>• Input Voltage: 320 V</li> <li>• Duty Cycle: 0.47</li> </ul>	
<i>Resonant Circuit:</i>		
<ul style="list-style-type: none"> <li>• Series Capacitor: 190 nF</li> <li>• Series Inductance: 5 μH</li> <li>• Volume CS + CP: 47.2 cm<sup>3</sup></li> </ul>	<ul style="list-style-type: none"> <li>• Parallel Capacitor: 490 nF</li> <li>• Turns Ratio: 7</li> <li>• Primary Turns: 14</li> </ul>	

Table 1. Optimal converter design for parameter range of Fig. 17

Further results of the optimisation procedure for different design specifications, materials and constraints will be presented in a future paper.

## 5. Conclusion

In this paper an analytic model for the series-resonant converter including the magnetic device is presented. This model includes also a ZCS condition for one leg of the converter and the control of the converter by frequency and duty cycle. The calculated results of the analytic model and for the flux distribution within the magnetic core correspond very well with the simulation and the measurement results presented for different resonant circuits.

With the presented analytic model it is possible to calculate the operating frequency, the duty cycle, all the currents and voltages and the flux distribution in the transformer for given input voltage, load resistance, load offset voltage and output current. The required calculation time for the model is low, so that the model could be used in the presented automatic optimisation procedure which optimises, for example, the overall converter volume or the efficiency of the converter system.

Within the optimisation procedure the losses in the transformer, the capacitors and the semiconductor are calculated and the (integrated) magnetic device is optimised in an inner optimisation loop and the overall converter volume in a second optimisation algorithm. A telecom power supply is designed with the proposed analytic model and optimisation procedure and the resulting design of the supply is presented (Output Power: 3.9kW, Overall converter Volume: 1.36dm<sup>3</sup>, Efficiency: 93% and Power Density: 2.85 kW/dm<sup>3</sup>).

## References

- [1] G. A. Ward, A. J. Forsyth, "Topology selection and design trade-offs for multi-kW telecom DC power supplies", *International Conference on Power Electronics, Machines and Drives*, No. 487, June 4-7, 2002, pp. 439 -444
- [2] F. Cavalcante, J. W. Kolar, "Design of a 5kW high output voltage series-parallel resonant DC-DC converter", *34<sup>th</sup> Power Electronics Specialist Conference*, Vol. 4, June 15-19, pp. 1807 -1814
- [3] S. Dieckerhoff, M. J. Ruan, R. W. De Doncker, "Design of an IGBT-based LCL-resonant inverter for high-frequency induction heating", *Conference Record of 34<sup>th</sup> Industry Applications Conference*, Vol. 3, Oct. 3-7, 1999, pp. 2039 - 2045
- [4] A. K. S. Bhat, S. B. Dewan, "Analysis and design of a high-frequency resonant converter using LCC-type commutation", *IEEE Transaction on Power Electronics*, vol.2, No.4, 1987, pp. 291-300
- [5] R. L. Steigerwald, "A comparison of half-bridge resonant converter topologies", *IEEE Transactions on Power Electronics*, Vol. 3, Issue: 2, April, 1988 pp. 174 -182
- [6] A. J. Forsyth, G. A. Ward, S. V. Mollov "Extended fundamental frequency analysis of the LCC resonant converter", *IEEE Transactions on Power Electronics*, Vol. 18, Issue 6, Nov., 2003, pp. 1286 - 1292
- [7] J. T. Strydom, "Electromagnetic design of integrated Resonator-Transformers", *Ph.D. Thesis, Rand Afrikaans University*, South Africa, 2001
- [8] M. C. Smit, J. A. Ferreira, J. D. van Wyk, "Application of transmission line principles to high frequency power converters", *23<sup>rd</sup> Power Electronics Specialists Conference*, Vol. 2, 29 June-3 July, 1992, pp. 1423 -1430

- [9] I. W. Hofsjager, "On electromagnetic integration in hybrid electronic structures", *D. Eng. Thesis, Industrial and Electronics Research Group*, Faculty of Engineering, Rand Afrikaans University, May 1998
- [10] J. Biela, J. W. Kolar, "Electromagnetic integration of high power resonant circuits comprising high leakage inductance transformers", *35<sup>th</sup> Power Electronics Specialists Conference*, June 20-25, 2004, pp. 4537 -4545
- [11] A. F. Witulski, "Introduction to modelling of transformers and coupled inductors", *IEEE Transactions on Power Electronics*, Vol. 10, Issue 3, May, 1994, pp. 349-357
- [12] A. Balakrishnan, W. T. Joines, T. G. Wilson, "Air-Gap reluctance and inductance calculations for magnetic circuits using Schwarz-Christoffel Transformation", *IEEE Transactions on Power Electronics*, Vol. 12, Issue 4, 1997, pp. 654-663
- [13] R. C. Roters, "Electromagnetic Devices", John Wiley & Sons, 1941
- [14] A. F. Hoke, C. R. Sullivan, "An improved two-dimensional numerical modelling method for E-Core Transformers", *17<sup>th</sup> Applied Power Electronics Conference and Exposition*, Vol. 1, March 10-14, 2002, pp. 151 - 157
- [15] C. P. Steinmetz, "On the law of hysteresis", *Proc. IEEE*, vol. 72, February 1984, pp. 196-221

**Jürgen Biela** (Non-member) was born in Nuremberg, Germany, on July 12, 1974.



He studied electrical engineering at the Friedrich-Alexander-Universität Erlangen. During his studies he dealt in particular with resonant DC-link inverters at the Strathclyde University, Scotland and the active control of series connected IGBTs at the Technical University of Munich, Germany. After he had received his diploma degree with honours from FAU Erlangen in October 2000, he worked on inverters with very high switching frequencies, SiC components and EMC at the research department of A&D Siemens, Germany. Since July 2002 he is Ph.D. student at the PES, ETH Zurich. His current

research is focused on electromagnetic integration of passive components and modelling, design and optimisation of DC-DC converters.

**Johann W. Kolar** (Member) studied industrial electronics at the University of Technology Vienna, Austria, where he also received the Ph.D. degree (summa cum laude). From 1984 to 2001 he was with the University of Technology in Vienna, where he was teaching and working in research in close collaboration with the industry in the fields of high performance drives, high frequency inverter systems for process technology and uninterruptible power supplies. He has proposed numerous novel converter topologies, e.g., the VIENNA Rectifier and the Three-Phase AC-AC Sparse Matrix Converter concept. Dr. Kolar has published over 150 scientific papers in international journals and conference proceedings and has filed more than 50 patents. He was appointed Professor and Head of the Power Electronics Systems Laboratory at the Swiss Federal Institute of Technology (ETH) Zurich on Feb. 1, 2001.



The focus of his current research is on novel AC-AC and AC-DC converter topologies with low effects on the mains for telecommunication systems, More-Electric-Aircraft applications and distributed power systems utilizing fuel cells. A further main area of research is the realization of ultra-compact intelligent converter modules employing latest power semiconductor technology (SiC) and novel concepts for cooling and EMI filtering.

Dr. Kolar is a Senior Member of the IEEE and a member of the IEEJ and of Technical Program Committees of numerous international conferences in the field (e.g. Director of the Power Quality branch of the International Conference on Power Conversion and Intelligent Motion). From 1997 through 2000 he served as an Associate Editor of the IEEE Transactions on Industrial Electronics and since 2001 as an Associate Editor of the IEEE Transactions on Power Electronics.